Angle-resolved electron-energy-loss spectroscopy of two-dimensional plasmons

J. I. Gersten
Department of Physics, The City College of the City University of New York, New York, New York 10031

I. Wagner, A. Rosenthal, Y. Goldstein, and A. Many
Racah Institute of Physics, The Hebrew University of Jerusalem, Jerusalem 91904, Israel

R. E. Kirby
Stanford Linear Accelerator Center, P.O. Box 4349, Stanford, California 94305
(Received 2 May 1983; revised manuscript received 8 September 1983)

Angle-resolved electron-energy-loss spectroscopy from solid-state surfaces is studied both theoretically and experimentally, with particular emphasis on the ZnO surface. The plasmonlike loss peak is found to shift as a function of detector angle. This is due to the highly dispersive nature of the plasmon mode. There is also evidence for a phononlike model which remains unshifted as a function of detector angle. The role of both collective and single-particle excitations are considered, and the theory is found to be in good agreement with the experiment.

I. INTRODUCTION

Two-dimensional space-charge layers on the surface have been studied extensively in the last decade or so.[1,2] The utility of such electron layers has perhaps best been illustrated by novel recent experiments on the quantized Hall effect.[3,4] The main thrust of the experimental effort relating to quantized electron layers has centered on the metal-oxide-semiconductor devices using silicon. In such devices the experimental techniques available to study the silicon surface, however, are restricted to optical probes or transport measurements. On ZnO, on the other hand, strong quantized accumulation layers can be obtained on the *free* surface, which is accessible to an electron-beam probe as well. In this paper we describe studies of such a surface by means of low-energy electron-energy-loss spectroscopy (LEELS).

The LEELS spectrum of the ZnO surface exhibits[5] a prominent surface-phonon energy-loss peak, as well as loss peaks corresponding to multiple phonon excitations. These peaks were also observed in our earlier studies[6] and were found to disappear as the accumulation layer on the surface was formed. In their place new loss peaks appeared which increased in energy as the strength of the accumulation layer was increased.[7] These peaks were attributed to two-dimensional plasmons of the accumulation layer.

The primary interest of our past work has been on specular scattering. However, some preliminary data have been reported on off-specular scattering[8] in which it was noted that the energy position of the dominant loss peak varied as a function of the scattering angle departure from specularity. The quantitative interpretation of this data has not yet been presented. One of the main goals of this paper is to present such a detailed theoretical interpretation.

The two-dimensional plasmon has a dispersion curve which emanates from the origin of the frequency—wave-vector plane (ω-$k_{||}$ plane) and monotonically increases in frequency with increasing wave vector. At some value of $k_{||}$ the plasmon curve intersects the phonon curves. The phonon and plasmon modes couple and the new hybrid modes that result have been termed surface plasmarons.[9] The plasmaron modes, labeled ω_+, ω_0, and ω_- are just linear combinations of the original phonon and plasmon modes. Extensive graphs of the dispersion curves for the plasmarons appear elsewhere in the literature[9] and so will not be repeated in this paper. At small $k_{||}$ the ω_- mode is plasmonlike, whereas the ω_0 and ω_+ modes are phononlike. At large $k_{||}$ ω_+ becomes plasmonlike while ω_- and ω_0 become phononlike. In the crossing region the characters of the modes are scrambled. The significance of the existence of such modes lies in the fact that one set of energy-loss channels for electron scattering stems from the excitation of the surface plasmarons. Expressions for the energy dispersions and coupling constants for these modes have been derived in the literature.[9]

Another potentially important energy-loss channel consists of driving the interband transition in which an electron of the accumulation layer is promoted from one quantized subband to another. Interestingly, the energy loss for this process falls roughly in the same range as the energy loss to the ω_+ plasmaron mode. The calculation of the interband contribution is presented in the Appendix. It is found to be much weaker than the corresponding contribution due to the collective excitations.

The plasmaron modes $\omega_\pm$ are highly dispersive in character, i.e., their frequencies are strongly varying functions of wave vector. In LEELS it is possible to observe a particular wave-vector excitation by appropriately choosing the angle that the detector makes with the specular direction. By virtue of conservation of momentum parallel to

the surface, a direct connection exists between the momentum loss of the electron and the momentum imparted to the excitation. Thus, in principle, it should be possible to map out the dispersion curves of the plasmaron branches by varying the detector angle and noting the positions of the LEELS peaks. In practice, however, this direct approach proves to be too ambitious. The kind of angular resolution required for such a measurement would be more than an order of magnitude less than the already excellent resolution of our instrument ($\sim 1°$). In addition, the crystal sample would need to have near perfect specularity. We therefore adopt an alternate, but equally valid, approach to the problem. We employ the theoretical dispersion curves and coupling constants as inputs to a scattering formalism and compare the resulting theoretical curves with experiment.

It should perhaps be noted that LEELS provides really the only direct way to measure the ω-$k_{||}$ dispersion relation for a free surface. While very elegant methods have been devised involving optical measurements and superimposed gratings for measuring the surface-plasmon dispersion relation, the imposition of a grating in a case where there is an accumulation layer is likely to perturb the free surface.

One of the simple predictions of the plasmaron model is that the ω_0 mode is not highly dispersive. Its frequency always lies in the vicinity of the surface- and bulk-phonon frequencies. The peak associated with the ω_0 branch, therefore, should not move noticeably with the detuning of the detector from the specular angle. As we shall see, this prediction is borne out experimentally. The situation concerning the ω_- mode, however, is not as fortunate. Its energy is low and it cannot be resolved from the elastic peak which, of course, is centered around zero energy electron loss.

Our work also shows an interesting correlation between the mobility of the sample and our ability to discern a well-defined plasmon peak. This trend has been empirically noted in our experiments over the years. In our early experiments, in which the mobility of the samples were low, the plasmon peak was difficult to observe, and in some cases simply blended into a coarse background. In our later experiments the mobility was improved, as was evidenced by direct transport measurements. We shall argue that the lifetime broadening of the plasmarons stems from the same collisional relaxation processes that contribute to the electron's mobility. Our theoretical analysis will show that only for sufficiently small broadening is a plasmon peak observable.

The paper is organized as follows. In Sec. II we consider the theory of LEELS as applied to a semiconductor surface. In Sec. III details of the experimental apparatus are described. This is followed by a comparison between theory and experiment in Sec. IV and finally a discussion in Sec. V. Details of the role of interband transitions are given in the Appendix.

II. THEORY

The purpose of this section is to develop a theory for low-energy electron-energy-loss spectroscopy (LEELS) from polar semiconductor surfaces. The theory is an extension of work previously reported in the literature.[10] The semiconductor will be assumed to possess an accumulation layer near its surface, with the electrons in this layer organized into quantized subbands. The inelastic processes contributing to the scattered electron's energy loss involve both collective surface excitations, including plasmons and phonons, and one-electron processes, such as interband transitions induced within the manifold of quantized subbands.

In order to calculate the probabilities for the various inelastic processes we will employ first-order perturbation theory. The unperturbed states correspond to incoming or outgoing plane-wave states modified by the presence of the surface. The interaction of the scattering electron with the surface excitation constitutes the perturbation. In formulating an expression for the unperturbed states we simplify matters by assuming that the surface acts to partially reflect and partially transmit electrons. Thus the incoming state is

$$\psi = (e^{ip_z z} + Re^{-ip_z z}) e^{i\vec{p}_{||}\cdot\vec{r}} \Theta(-z) + Te^{i(q_z z + \vec{p}_{||}\cdot\vec{r})} \Theta(+z) , \tag{1}$$

where the crystal occupies the half-space $z > 0$. Here p_z denotes the component of momentum directed perpendicular to the surface, $\vec{p}_{||}$ is the momentum vector projected parallel to the surface, and R and T are the reflection and transmission amplitudes, respectively. The normal component of the momentum within the crystal is denoted by q_z. We will work in atomic units ($\hbar = e = m = 1$). The state represented by Eq. (1) is somewhat inadequate in that it neglects the Bloch nature of the wave functions within the crystal. This deficiency, and its consequences, will be discussed later. The electronic energy is

$$\epsilon = \tfrac{1}{2}(p_z^2 + p_{||}^2) . \tag{2}$$

In a similar way the outgoing state ψ' is given by

$$\psi' = (e^{ip_z' z} + R'^* e^{-ip_z' z}) e^{i\vec{p}'_{||}\cdot\vec{r}} \Theta(-z) + T'^* e^{i(q_z' z + \vec{p}'_{||}\cdot\vec{r})} \Theta(+z) , \tag{3}$$

where now the final electron energy is

$$\epsilon' = \tfrac{1}{2}(p_z'^2 + p_{||}'^2) . \tag{4}$$

For an inelastic process ϵ' and $\vec{q}'_{||}$ will be different from ϵ and $\vec{q}_{||}$. The differences are taken up by the surface excitation.

As mentioned in the Introduction, the basic surface modes of a semiconductor consist of coupled surface plasmons and phonons, and are referred to as surface plasmarons. The frequencies of these excitations are denoted by $\omega_\lambda(K_{||})$, where $\vec{K}_{||}$ is the wave vector parallel to the surface and λ is an index assuming the values -1, 0, and 1. The interaction of an electron with the plasmarons is described by the second-quantized Hamiltonian

$$H_1 = -\sum_{\vec{K}_{||},\lambda} \gamma_\lambda(\vec{K}_{||})[a_\lambda(\vec{K}_{||}) f_\lambda(\vec{K}_{||},z) e^{i\vec{K}_{||}\cdot\vec{r}} + \text{H.c.}] , \tag{5}$$

where $\gamma_\lambda(K_{||})$ is a generalized Frohlich coupling constant, $a_\lambda(\vec{k}_{||})$ is an annihilation operator, and $f_\lambda(\vec{k}_{||},z)$ describes the spatial profile of the plasmaron excitation in the z direction. Examples for the dispersion curves $\omega_\lambda(K_{||})$ and coupling constants $\gamma_\lambda(K_{||})$ for ZnO have appeared in the literature.[6-9] In the vacuum region $f(\vec{k}_{||},z)=\exp(k_{||}z)$ while in the crystal region it is generally a more complicated function of space. However, in the limit of a thin accumulation layer we may write $f(\vec{k}_{||},z) = \exp(-k_{||}|z|)$ which is then valid in all space. The conclusions to be drawn using this formula, however, are more general than for the case of just thin accumulation layers.

The matrix element for inelastic electron excitation of a plasmaron in the lowest order of perturbation theory is

$$\langle \psi';\vec{K}_{||},\lambda | H_1 | \psi;\text{vac}\rangle = -(2\pi)^2\delta(\vec{p}\,'_{||}+\vec{K}_{||}-\vec{p}_{||})\gamma_\lambda(\vec{K}_{||})[n_\lambda(K_{||})+1]^{1/2} \times \left[\frac{1}{K_{||}+i(p_z-p_z')} + \frac{R}{K_{||}-i(p_z+p_z')} + \frac{R'}{K_{||}+i(p_z+p_z')} + \frac{RR'}{K_{||}+i(p_z'-p_z)} + \frac{TT'}{K_{||}+i(q_z'-q_z)} \right] , \tag{6}$$

where $n_\lambda(k_{||})=[\exp(\beta\hbar\omega)-1]^{-1}$ is the surface plasmaron occupancy factor. Noting that $p_z>0$ and $p_z'<0$, we conclude that Eq. (6) contains terms that are "resonant," in that the denominator may be small, and terms that are "antiresonant," in that the denominator will be large. The matrix element will be dominated by the former terms and may be reexpressed as

$$\langle \psi';\vec{K}_{||},\lambda | H_1 | \psi,\text{vac}\rangle = -(2\pi)^2\delta(\vec{p}\,'_{||}+\vec{K}_{||}-\vec{p}_{||})\gamma_\lambda(\vec{K}_{||})[n_\lambda(\vec{K}_{||})+1]^{1/2}\frac{2K_{||}R}{K_{||}^2+(p_z+p_z')^2} . \tag{7}$$

We have introduced the added assumption that the energy loss is sufficiently small compared with the primary electron energy that $R'\approx R$.

The rate for an inelastic process in which a plasmaron is produced is given by Fermi's golden rule. If we divide this rate by the probability of an electron being reflected, $|R|^2$, and by the incident flux of electrons, we obtain an expression for the probability that a reflected electron has excited a surface plasmaron. Expressing the momentum volume element as $d\vec{p}\,' = p'^2 dp' d\Omega'$ we may write the differential probability for plasmaron excitation as

$$\frac{dp}{d\epsilon' d\Omega'} = \frac{1}{\pi^2}\frac{p'}{p}\sum_\lambda |\gamma_\lambda(K_{||})|^2 \frac{[n_\lambda(K_{||})+1]K_{||}^2}{[K_{||}^2+(p_z+p_z')^2]^2}\delta(\epsilon-\epsilon'-\omega_\lambda(K_{||})) . \tag{8}$$

Inclusion of lifetime broadening of the plasmarons is achieved in the Wigner-Weisskopf manner by replacing the Dirac δ function by a Lorentzian

$$\delta(\epsilon-\epsilon'-\omega_\lambda(K_{||})) \rightarrow \frac{\sigma_\lambda(K_{||})}{\pi}\frac{1}{[\sigma_\lambda(K_{||})]^2+[\epsilon-\epsilon'-\omega_\lambda(K_{||})]^2} , \tag{9}$$

where $\sigma_\lambda(K_{||})$ is the half width at half maximum at the plasmaron resonance.

In the experimental situation of interest here, $\omega_\lambda(K_{||}) \ll \epsilon$ and so $p'\approx p$. The scattering geometry is illustrated in Fig. 1. Letting

$$\vec{p} = (2\epsilon)^{1/2}(\hat{i}\sin\theta + \hat{k}\cos\theta) , \tag{10a}$$

$$\vec{p}\,' = (2\epsilon)^{1/2}[(\hat{i}\cos\delta\phi + \hat{j}\sin\delta\phi)\sin\theta' - \hat{k}\cos\theta'] , \tag{10b}$$

where the angular deviations from specularity are

$$\delta\theta = \theta' - \theta , \tag{11a}$$

$$\delta\phi = \phi' , \tag{11b}$$

and an energy-loss parameter

$$\delta\epsilon = \epsilon - \epsilon' , \tag{11c}$$

we obtain, to leading order in $\delta\theta$, $\delta\phi$, and $\delta\epsilon/\epsilon$,

$$\frac{d^3\mathscr{P}}{d\epsilon' d\delta\theta d\delta\phi} = \frac{\sin\theta}{(2\pi\epsilon)^2}\sum_\lambda |\gamma_\lambda|^2 \frac{\sigma_\lambda}{\pi}\frac{n_\lambda+1}{\sigma_\lambda^2+(\delta\epsilon-\omega_\lambda)^2}\frac{K_{||}^2}{\left[(\sin\theta\,\delta\phi)^2+(\delta\theta)^2+\left[\frac{\delta\epsilon}{2\epsilon}\right]^2\right]^2} . \tag{12}$$

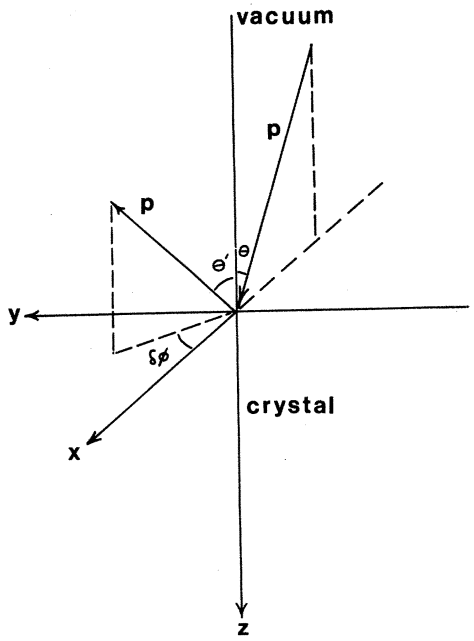

FIG. 1. Scattering geometry. The incident (outgoing) electron momentum is denoted by $\vec{p}$ ($\vec{p}\,'$). Likewise θ and θ' denote the angles of incidence and reflection, respectively. The azimuthal deflection is denoted by $\delta\phi$.

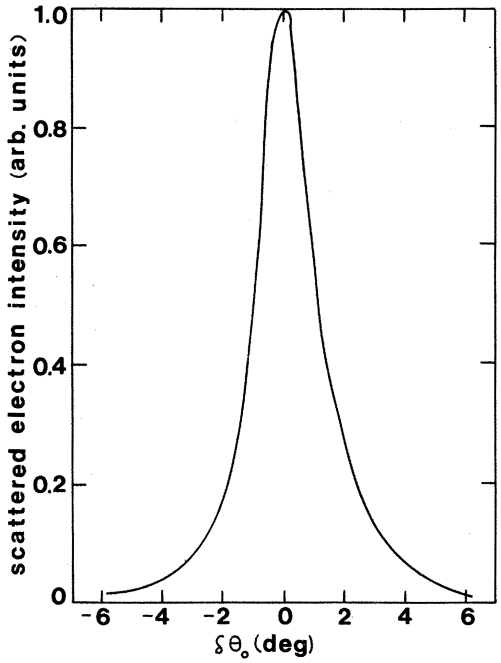

FIG. 2. Typical angular dependence of the elastically scattered beam.

Here we have

$$K_{||}=\left\{2\epsilon\left[(\sin\theta\,\delta\phi)^2+\left[\delta\theta\cos\theta-\frac{\delta\epsilon}{2\epsilon}\sin\theta\right]^2\right]\right\}^{1/2} \tag{13}$$

and

$$p_z+p_z'=(2\epsilon)^{1/2}\left[\sin\theta\,\delta\theta+\frac{\delta\epsilon}{2\epsilon}\cos\theta\right]. \tag{14}$$

In the actual experiments the angular resolution of the detector is finite and the specularity of the crystal is nonperfect. Both of these effects may be taken into account by introducing an angular resolution function

$$F(\delta\theta,\delta\phi)=\exp\left[-\frac{1}{\Delta\theta}[(\delta\theta-\delta\theta_0)^2+(\sin\theta\,\delta\phi)^2]^{1/2}\right], \tag{15}$$

where $\Delta\theta$ is the experimental angular resolution and $\delta\theta_0$ is the angular setting of the detector measured from the specular direction. This function is peaked around $(\delta\theta,\delta\phi)=(\delta\theta_0,0)$ and has wings which fall off exponentially with increasing deviation of the scattered beam from the detector setting. The observed plasmaron loss signal is obtained by integrating the product of Eqs. (12) and (15) over angles:

$$\left.\frac{d\mathcal{P}}{d\epsilon'}\right|_{\text{plasmaron}}=\int d(\delta\theta)\int d(\delta\phi)F(\delta\theta,\delta\phi)\times\frac{d^3\mathcal{P}}{d\epsilon'd(\delta\theta)d(\delta\phi)}. \tag{16}$$

The elastically scattered beam has a simple expression in place of Eq. (12),

$$\left.\frac{d^3\mathcal{P}}{d\epsilon'd(\delta\theta)d(\delta\phi)}\right|_{\text{elastic}}=\delta(\delta\epsilon)\delta(\delta\theta)\delta(\delta\phi), \tag{17}$$

so that corresponding to Eq. (16) we have

$$\left.\frac{d\mathcal{P}}{d\epsilon'}\right|_{\text{elastic}}=\delta(\delta\epsilon)\exp\left[-\frac{|\delta\theta_0|}{\Delta\theta}\right]. \tag{18}$$

The finite energy resolution of the detector is taken into account by averaging Eqs. (16) and (18) over the resolution function

$$G(\epsilon_0',\epsilon')=\frac{1}{\Delta\epsilon(2\pi)^{1/2}}\exp\left[-\frac{1}{2}\left[\frac{\epsilon_0'-\epsilon'}{\Delta\epsilon}\right]^2\right], \tag{19}$$

where $\Delta\epsilon$ is a measure of the detector's energy width, and ϵ_0' is the energy setting of the detector. Note that in the particular case where $\Delta\epsilon\ll\sigma_\lambda$, $G(\epsilon_0'-\epsilon')$ reduces to a Dirac δ function and the energy average is not necessary.

Figure 2 illustrates a typical angular dependence of the elastically scattered beam. A fit of the parameters $\Delta\theta$ and $\Delta\epsilon$ appearing in Eqs. (15) and (19) to typical experimental data gives 1° and 0.015 eV.

In order to understand the limitations of our previously derived formula Eq. (12), let us rederive it using first-order time-dependent perturbation theory. Let us consider the classical trajectory

$$\vec{r}=\vec{v}_{||}t+v_z\hat{k}\,|\,t\,|\,. \tag{20}$$

Here the trajectory is assumed to consist of two straight line segments with the collision occurring at time $t=0$. The amplitude for plasmon excitation is given by

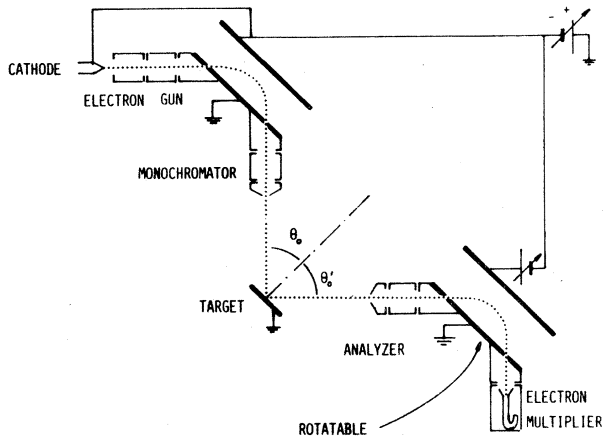

FIG. 3. Experimental arrangement.

$$S=i\gamma_\lambda(\vec{K}_{||})\int_{-\infty}^{\infty}dt\exp[i(\omega-\vec{K}_{||}\cdot\vec{v}_{||})t-K_{||}v_z\,|\,t\,|\,]$$
$$=\frac{2iK_{||}v_z\gamma_\lambda(K_{||})}{(K_{||}v_z)^2+(\omega-\vec{K}_{||}\cdot\vec{v}_{||})^2}\,. \tag{21}$$

The probability for plasmaron excitation caused by this pulse of interaction with the classical electron is

$$d^3\mathscr{P}=|S|^2\frac{d^2K_{||}}{(2\pi)^2}\delta(\delta\epsilon-\omega)d(\delta\epsilon)\cos\theta\,. \tag{22}$$

(The additional factor $\cos\theta$ is caused by an ambiguity in the semiclassical formulation and is needed in order to get agreement between the semiclassical and quantum formulas.) Using the fact that $d^2K_{||}=d^2p'_{||}$ and the formulas

$$(K_{||}v_z)^2=(2\epsilon\cos\theta)^2\left[(\sin\theta\,\delta\phi)^2+\left[\frac{\delta\epsilon}{2\epsilon}\sin\theta-\cos\theta\,\delta\theta\right]^2\right] \tag{23}$$

and

$$(\omega-\vec{K}_{||}\cdot\vec{v}_{||})^2=(2\epsilon\cos\theta)^2\left[\frac{\delta\epsilon}{2\epsilon}\cos\theta+\sin\theta\,\delta\theta\right]^2, \tag{24}$$

we obtain Eq. (12) in the semiclassical limit.

From the above, we see that the quantum theoretical result is equivalent to the semiclassical result for a classical trajectory which never penetrates the crystal. In reality, however, one expects penetration to occur. The role of penetration effects in low-energy electron diffraction has been considered in the literature.[11] The incident electron may penetrate the lattice and be reflected from a bulk ion or may undergo a succession of collisions before emerging from the crystal. This would have an affect on the magnitude of the integral appearing in Eq. (21) since it lengthens the time of interaction between the incident electron and the plasmaron wave.

One may envisage several limiting cases. If the penetration depth of the electron were large compared with the typical plasmaron size, $K_{||}^{-1}$, the amplitude of Eq. (21) would be twice that previously found and the inelastic scattering probability would have to be multiplied by a factor of 4. However, this assumes that the scattering electron does not undergo phase interrupting collisions in the course of its trajectory. If it does undergo such dephasing collisions, the coherence is broken and the probabilities should be added rather than the amplitudes, and an enhancement of only a factor of 2 will result. In our calculations we shall introduce this factor of 2 as a phenomenological correction for penetration.

In addition to plasmaron excitation we also wish to calculate the contribution of interband transitions to the scattering probability. An analysis of these transitions is presented in the Appendix.

III. EXPERIMENTAL

The measurements were carried out on the "oxygen" (0001) face of ZnO crystals grown by the Airtron Company using the hydrothermal method. The samples were cut to typical dimensions of $10\times5\times1$ mm^3 with the hexagonal c axis perpendicular to the large surfaces. The surface was lapped with aluminum powder to a flatness of 0.1 μm, etched in concentrated HCl and then chemically polished in a 2% bromine-methanol solution. For current contacts we used tantalum pressure contacts upon sputtered vanadium. For voltage probes (four-contact method) tungsten pressure contacts were used. The sample was mounted in an ultrahigh vacuum chamber between two metal posts which also served as current leads. The surface cleaning cycle consisted of repeated argon bombardment at a pressure of 1 mTorr while keeping the sample at a temperature of 200 °C, and annealing at 500 °C. Accumulation layers were produced by exposure to atomic hydrogen.[12–14] To destroy the accumulation layer the surface was exposed to oxygen.

Because the surface mobility μ could not be measured in the present configuration, we use the values of μN_s to characterize our accumulation layers. These values, in turn, were derived from the measured surface conductance assuming that the "zinc" and "oxygen" faces contribute equally to the conductance. Actually, however, we have no way of estimating the relative contribution of each of the polar faces, so that the values quoted below for μN_s should be taken merely as qualitative indications of the strength of the quantized accumulation layer. Accordingly, in all subsequent comparisons between theory and experiment N_s will be taken as an adjustable parameter. We estimate that our highest experimental N_s values were around $(7-10)\times10^{13}$ cm^{-2}.

The LEELS measurements were performed in a vacuum of 10^{-9} Torr. The experimental arrangement is shown schematically in Fig. 3. An electron gun, consisting of a negatively biased cathode and electrostatic lenses, feeds electrons at 45° into a plane parallel high-resolution monochromator. The electrons impinge on the crystal at an angle θ_0 with the normal to the surface and the scattered electrons are collected at an angle θ'_0. The scattered electrons are energy resolved while passing through the analyzer. This is accomplished by changing the voltage across the analyzer plates. The emerging electrons are

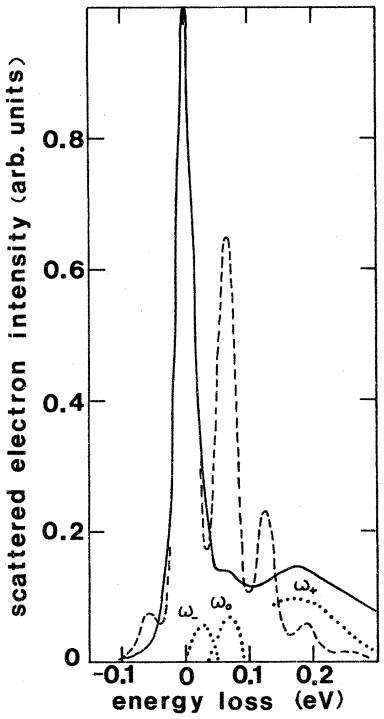

FIG. 4. Electron intensity for specular scattering as a function of energy loss. The dashed curve is experimental data for the bare ZnO surface with $\theta_0=\theta_0'=55°$ and $\epsilon=9.5$ eV. The solid curve is data for ZnO with an accumulation layer of electrons characterized by $\mu N_s=13\times10^{15}$ (V sec)$^{-1}$. The dotted curves represent the theoretical contributions from ω_-, ω_0, and ω_+ plasmarons for $N_s=3\times10^{13}$ cm^{-2}.

then detected by the channel electron multiplier. In the schematic of Fig. 3, $\theta_0'=\theta_0$, i.e., the specular beam is collected. However, both the analyzer and the crystal can be rotated and thus θ_0 and θ_0' can be varied independently. For angle dependence measurements usually θ_0 was kept constant and θ_0' was varied.

IV. RESULTS

The dramatic change in the energy-loss spectrum from the ZnO surface brought about by electrons in a surface accumulation layer is demonstrated by Fig. 4. The incident electron energy here is 9.5 eV and the incident angle $\theta_0=55°$. The scattered electron intensity is measured at specular reflection ($\delta\theta_0=0$). The oxygen ZnO surface has been ion bombarded and annealed, as described above. The dashed curve is the loss spectrum in the absence of electrons ($N_s=0$). The peak at zero-energy loss corresponds to elastic scattering. The pronounced loss peak at $\sim$65 meV corresponds to the unperturbed (bare) surface phonon.[6,10] The peaks at higher loss energies involve two-, three-, and four-phonon processes. Also seen is the anti-Stokes peak (at about -65 meV) representing an absorption of a thermal surface phonon by the scattered electron. The solid curve in the figure represents the loss spectrum after a quantized accumulation layer has been produced at the surface by exposure to atomic hydrogen. The pronounced peak at 65 meV is seen to have almost completely disappeared, leaving a weak shoulder at about the same energy. This shoulder is attributed to ω_0, the coupled plasmon—bulk-phonon—surface-phonon mode. [In ZnO the bulk phonon energy ($\sim$72 meV) should be very close to the (bare) surface phonon energy ($\sim$68 meV).] In addition a new loss peak at $\sim$175 meV appears. This peak is considerably broader than the phonon peaks and is attributed to the ω_+ plasmaron. The dotted curve represents calculated loss spectra originating from the ω_-, ω_0, and ω_+ plasmaron branches. The calculations are based on the value of $N_s=3.0\times10^{12}$ cm^{-2}. As has been pointed out above, the surface electron density in the accumulation layer, N_s cannot be determined accurately, and this value has been chosen so as to be compatible with the observed energy position of the peak. For the sake of clarity the strong elastic signal has been omitted in the calculated curves. It is seen that the ω_- contribution is unresolvable experimentally because with our available resolution it is masked by the elastic peak. On the other hand, the ω_0 and ω_+ contributions are clearly observed and account well for the shape of the experimental curve. The displacement of the experimental curve upwards with respect to the theoretical curves is believed to be caused by background scattering originating from large $k_{||}$ processes associated with surface roughness (see Sec. V).

Figure 5 represents a series of measured loss spectra for different accumulation layers, again at specular reflection. It is clearly seen that, as expected, the loss shoulder at 65—70 meV, attributed to ω_0, does not shift, whereas the ω_+ broad peak shifts to higher energies the stronger the accumulation layer (larger μN_s). The inset demonstrates a theoretical fit with one of the experimental curves (C) this time including the elastic peak.

So far we have considered energy-loss spectra at specular reflection. The solid curves in Fig. 6 represent data obtained at different off-specular angles on one and the same surface accumulation layer. Figure 6(a) corresponds to "negative angles," i.e., $\theta_0'<\theta_0$ (analyzer rotated towards the monochromator with respect to its specular position—see Fig. 3), whereas Fig. 6(b) corresponds to "positive angles," $\theta_0'>\theta_0$. The bottom curves in both Figs. 6(a) and 6(b) were obtained for specular reflection and are similar to those presented in Figs. 4 and 5. The scattered electron intensity is normalized with respect to the elastic peak (at zero energy loss). For the off-specular data the base line has been shifted upwards to facilitate the presentation. It should be noted that here, as well, the scattered intensity at each off-specular angle, has been normalized with respect to the elastic intensity at that angle. It is seen that for both negative and positive angles the plasmaron ω_+ peak shifts to higher energies the larger the off-specular angle. This is just as expected since a larger angle corresponds to a larger $K_{||}$ and hence to higher ω_+. The dashed curve in each case represents the calculated normalized scattered intensity for $N_s=3.5\times10^{13}$ cm^{-2}. N_s was taken as the only adjustable parameter in the calculations and represents the best fit for all scattering angles. This fit is seen to be quite good both as regards the positions and the shapes of the loss peaks. Here again, the theoretical curves lie below the ex-

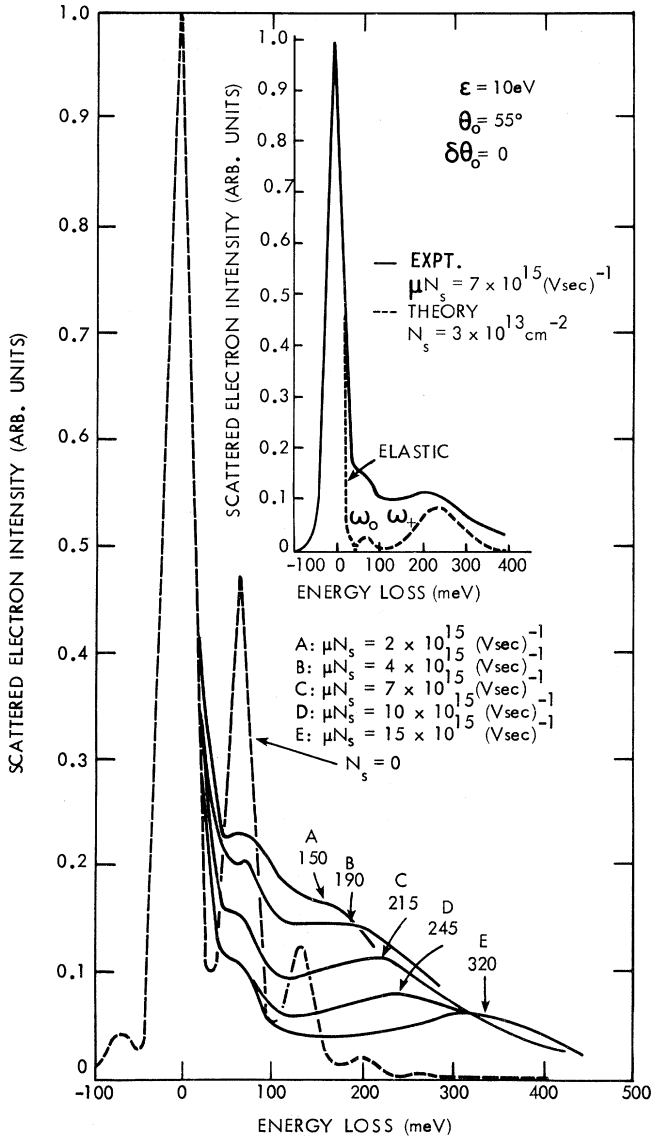

FIG. 5. Electron intensity for specular scattering as a function of energy loss for several accumulation layers. The $N_s=0$ curve is presented along with data for five accumulation layer cases, labeled $A-E$. The values of μN_s and the peak locations are given on the graph. The inset shows an example of the theory vs experiment for a particular case. Here no correction for penetration was included in the theoretical calculation.

perimental curves because of the background scattering not included in the theory (see Sec. V).

In Fig. 7 the points represent measured shifts in the energy position of the ω_+ loss peak with respect to its specular position as a function of the off-specular angle $\delta\theta_0$. The results have been obtained from measurements of the type shown in Fig. 5, taken for the same surface. The curve represents the theory for $N_s=3.5\times10^{13}$ cm^{-2}, the same value used in Fig. 6. It is interesting to note that, as expected from kinematical considerations, the energy shifts in Fig. 7 are asymmetrical with respect to specular angle ($\delta\theta_0=0$).

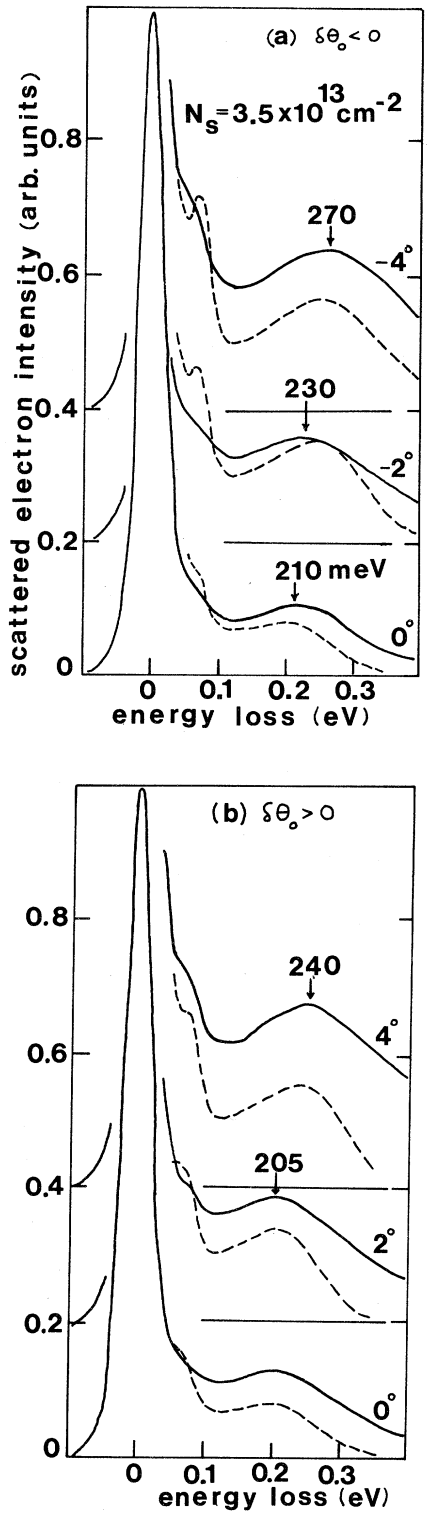

FIG. 6. Scattered electron intensity as a function of electron energy loss for several detuning angles away from specularity. The experimental data is shown by the solid lines while the theoretical curves are the dashed lines.

V. DISCUSSION

The primary focus of this paper is on the angular dependence of the LEELS spectrum. The spectrum is

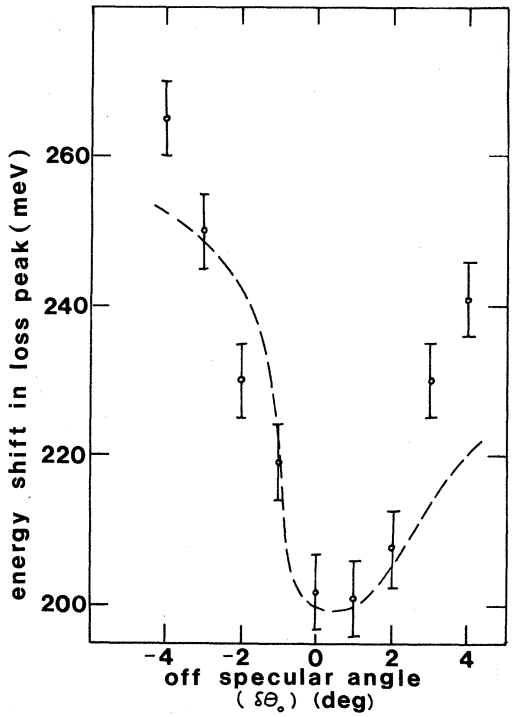

FIG. 7. Data points are the position of the loss peak for several detuning angles. The dashed curve is the theoretical prediction.

characterized by a strong elastic peak, a broad plasmon peak, and a phonon shoulder. In addition there is a broad background in the spectrum. As the angular deviation from specularity is increased the plasmon peak shifts towards higher energies whereas the phonon peak does not. Let us discuss qualitatively these various trends.

We have identified the high energy-loss peak with the ω_+ plasmaron mode, which, if sufficiently removed from the phonon mode, is plasmonlike. In order to assess the relative contribution of the interband $0\rightarrow 1$ transition, a calculation of the relative size of the LEELS spectra associated with plasmarons and interband transitions has been made. For $N_s=3.5\times 10^{13}$ cm^{-2} the peak of the interband spectrum was found to lie only 30 meV higher in energy loss than the peak of the plasmaron spectrum. However, the relative magnitudes of the interband and plasmaron spectra were found to be in the ratio 1:10. The widths were also comparable. Thus the interband contribution may, to a first approximation, be neglected in analyzing the experimental data.

One of our major goals of this work has been to verify the highly dispersive character of the ω_+ plasmaron and to show that the ω_0 plasmaron has no discernible dispersion. These trends are clearly illustrated in Fig. 6 where the ω_+ plasmaron peak shifts towards higher energies with increased detuning from specularity, whereas the ω_0 shoulder remains unshifted. As mentioned before the data in Fig. 6 cannot be immediately inverted to give a dispersion curve for ω_+ vs $K_{||}$. The reason for this is simple. An examination of Eq. (12) shows that the LEELS intensity is determined by two factors: a Lorentzian line-shape factor which is peaked around $\delta\epsilon=\omega(k_{||})$, and an angular form factor which is sharply peaked around the specular direction. The observed intensity is then obtained from Eq. (16) which involves integration against the detector resolution function. The detector resolution function, of course, is peaked around the value set by the monochromator and analyzer, $\delta\theta_0$, but has wings extending through a broad range of angles. At any given setting the detector samples contributions from both the Lorentzian line-shape factor and the angular form factor. The Lorentzian, in fact, does peak at the angle value determined by the dispersion curve, but the form factor peaks always in the specular direction. At larger detuning angles the relative contribution of the Lorentzian peak over the form factor peak increases and hence the peak location shifts as a function of detuning angle. In order to obtain the dispersion curves directly it would be necessary for the detector to have a very narrow angular acceptance, much more than is now possible, so as to be able to discriminate against the form factor contribution. Thus we are forced to attack the problem in the reverse direction. We must compute the theoretical curves and compare them directly with experiment, after having folded in the detector resolution function. The good agreement between theory and experiment vindicates this approach.

An examination of Eq. (12) shows that the tendency for the LEELS intensity to peak around the value determined by the dispersion curve diminishes as the plasmaron lifetime decreases. There are several possible causes of a finite plasmaron lifetime. First of all there is electron collisions with impurities or phonons. Plasmons are the cooperative oscillations of the electron gas. If an electron undergoes a collision a dephasing results which destroys the coherence of the plasmaron. Another possible mechanism for finite lifetime results from the creation of an electron-hole pair following an electron-electron collision. While such a process cannot occur for low-momentum change collisions, if there is microscopic roughness or impurities present, they can provide momentum kicks to the electron-electron system to enable such a process to proceed. Finally, one must consider the decay of the ω_+ plasmaron to a lower branch plasmaron (ω_0 or ω_-) and the creation of an electron-hole pair. Since some of these processes also contribute to the electrical resistivity of the sample let us estimate the parameter σ_λ appearing in Eq. (9) using the mobility. Using $\sigma=1/\tau=e/m^*\mu$ and a typical value of $\mu\approx 100$ cm^2/V s we find $\sigma\approx 40$ meV. In our numerical calculations we used $\sigma=35$ meV. If a value of 70 meV were used instead for σ it was found that the ω_+ plasmaron no longer manifested itself as a peak but only as an extended shoulder. Thus in order to see a well-defined plasmaron peak it is necessary that the mobility of the sample be sufficiently high. This trend was observed in our experiments: Only the high-mobility samples, as determined by transport measurements, exhibited a well-defined plasmaron peak.

From an examination of Fig. 6 we note that the plasmaron peaks are more pronounced for large $|\delta\theta_0|$ than they are for specular scattering. This may be understood as also being due to the finite lifetime, $1/\sigma_\lambda$. What determines the sharpness of a peak is the ratio $\omega_\lambda/\sigma_\lambda$; the

TABLE I. Parameters for ZnO accumulation layers extracted from D. Eger and Y. Goldstein, Phys. Rev. B 19, 1089 (1979). Here N_s is the surface electron concentration, L_c is the effective width of the accumulation layer, V_s is the surface barrier height, ϵ_n is the energy of the bottom of the nth subband, ϵ_F is the Fermi energy, and f_n is the fractional occupancy of the nth subband.

N_s ($\times 10^{13}$cm^{-2})	L_c (Å)	V_s (V)	ϵ_0 (eV)	ϵ_1 (eV)	ϵ_2 (eV)	ϵ_F (eV)	f_0	f_1
2	20	0.89	0.48	0.68	0.75	0.69	0.92	0.07
4	16	1.23	0.78	1.10	1.22	1.15	0.88	0.10
6	13	1.65	1.02	1.48	1.63	1.55	0.85	0.13
8	12	2.08	1.23	1.82	2.00	1.92	0.83	0.16
10	11	2.44	1.42	2.10	2.32	2.25	0.81	0.18

larger the ratio the sharper the peak. Since σ_λ remains fixed, whereas ω_λ increases as the detector is tuned away from specularity, we have an increased ω/σ ratio and hence a sharper peak. In addition the effect of the form factor, which weights in the specular direction, is reduced.

The actual width of the LEELS plasmaron peak is due to two factors. One is the lifetime width described by the parameter σ_λ. The second is due to the finite angular acceptance of the detector, $\Delta\theta$. By accepting a range of scattering angles, a range of wave vectors is simultaneously seen by the detector. Owing to the dispersion of the mode, this results in a substantial contribution to the width. Since experimentally we find that the width of the ω_+ mode exceeds the value of σ_λ we conclude that the detector width is probably the more important of the two effects.

The broad background that lies below the plasmaron peaks is, in part, due to electron-hole excitations that become possible due to surface roughness or impurities. Indeed the discrete nature of the Zn ions responsible for the existence of the accumulation layer could be the cause of this roughness. Additional evidence for the existence of these microscopic impurities comes from the nonspecularity of the sample. In the absence of an electron gas on the surface the broad background is also absent, as is evidenced by Figs. 4 and 5. By the same token the wave-vector components supplied by surface roughness or impurities can also permit a wider range of plasmons to be excited at a given electron wave-vector transfer $K_{||}$. It is observed that the existence of the background is independent of the detuning angle $\delta\theta_0$.

In contrast to the shift of ω_+ with detuning from specularity, the ω_0 peak is unshifted. The lack of shift results from the lack of dispersion of the ω_0 mode. This trend is seen both from the experimental data and from the theoretical calculations.

It is perhaps worthwhile, at this point, to summarize the experimental parameters that have entered our analysis. These are the following: (1) the angular resolution parameter, (2) the energy resolution of the instrument, and (3) the plasmon lifetime. The angular resolution of the instrument and the "rocking angle" of the nonspecular solid surface combine to give an effective angular resolution function for the experiment which is seen in Fig. 2. The angular half width at half maximum is seen to be about 1°. Likewise the energy resolution of the experiment may be deduced by examining the elastic peak of the scattered electron intensity data of Figs. 4 or 5. Finally, the plasmon lifetime is estimated from the experimental mobility data. The theoretical fits were not very sensitive to the precise values of these three parameters as they were varied over physically acceptable ranges.

Other than these experimentally available parameters the only adjustable parameter is N_s, the surface electron concentration. The choice of N_s is, in fact, quite critical. The degree of agreement between theory and experiment is sensitive to the choice of N_s since the location of the ω_+ peak is determined by it. Once a proper choice for N_s is made, it is possible to fit a whole family of curves, as was illustrated in Fig. 6.

In conclusion, we believe that the systematics of the LEELS spectra can be described in terms of the excitation of surface plasmarons.

ACKNOWLEDGMENTS

The authors wish to acknowledge support from the National Council for Research and Development, Israel, the Gesellschaft für Kernforschung Karlsruhe, Federal Republic of Germany, the U.S.—Israel Binational Science Foundation, and the PSC-BHE (Professional Staff Congress—Board of Higher Education) grant program of the City University of New York.

APPENDIX: INTERBAND TRANSITIONS

The electrons in the accumulation layer are organized into subbands which will be labeled 0, 1, 2, etc. Within a given subband the electronic states are described by a two-dimensional wave vector. Interband transitions between any of the subbands are possible. Since the fractional occupancy of state 1 is small, in most cases (see Table I), we only consider $0\rightarrow 1$ interband transitions.

We shall use time-dependent perturbation theory here. An electron moving along the trajectory $\vec{R}(t)$ interacts with a subband electron at position $\vec{r}$ by means of the interaction energy

$$\phi(\vec{r}) = -\frac{2}{1+\epsilon_c}\frac{1}{|\vec{r}-\vec{R}|}, \tag{A1}$$

where ϵ_c is the dielectric constant of the crystal. Since the dielectric function is frequency dependent, we must evaluate ϵ_c at some characteristic frequency. The typical scale for r is L_c, the effective width of the accumulation layer, and the speed of the scattering electron is v, so the characteristic frequency is $\omega_c \sim v/L_c$. An estimate of ω_c for a 9-eV electron and $L_c \sim 15$ Å gives $\hbar\omega_c = 0.78$ eV. Since this lies above the phonon and typical plasmon energies,

we will take $\epsilon_c=\epsilon_\infty=4$ the value appropriate to ZnO.

Let the wave function describing an electron in the ground subband with wave vector parallel to the surface $q_{||}$ be denoted by $\langle \vec{r}\,|\,\vec{q}_{||},0\rangle=\psi_0(z)\exp(i\vec{q}_{||}\cdot\vec{r})$. Similarly a first excited subband state may be written as $\langle \vec{r}\,|\,\vec{q}\,'_{||}1\rangle=\psi_1(z)\exp(i\vec{q}\,'_{||}\cdot\vec{r})$. The corresponding energies are $\epsilon_0+q_{||}^2/2m^*$ and $\epsilon_1+q_{||}'^2/2m^*$, respectively, where m^* is the effective mass of the electron at the bottom of the band ($m^*=0.28$ for ZnO). The amplitude for the $0\rightarrow1$ transition is

$$S=\frac{2i}{1+\epsilon_c}\int_{-\infty}^{\infty}dt\,e^{i\omega t}\int d\vec{r}_{||}\int_0^\infty dz\frac{\psi_1(z)\psi_0(z)}{|\vec{r}-\vec{R}(t)|}\times e^{i(\vec{q}_{||}-\vec{q}\,'_{||})\cdot\vec{r}_{||}}, \quad \text{(A2)}$$

where $\vec{R}(t)$ is given by Eq. (20) and now

$$\omega=\epsilon_1-\epsilon_0+(q_{||}'^2-q_{||}^2)/2m^* . \quad \text{(A3)}$$

Here ω represents the energy loss of the primary electron. The original electron in band 0 lies below the Fermi level, whereas the promoted electron in band 1 lies above it, i.e., $\epsilon_0+q_{||}^2/2m^*\le\epsilon_F\le\epsilon_1+q_{||}'^2/2m^*$. Evaluation of the spatial integral in Eq. (A2) gives

$$S=\frac{4\pi i\gamma}{K_{||}(1+\epsilon_c)}\int_{-\infty}^{\infty}dt\,e^{i\omega t+i\vec{K}_{||}\cdot\vec{R}_{||}+K_{||}R_z(t)}, \quad \text{(A4)}$$

where now

$$\gamma=\int_0^\infty dz\,\psi_1(z)\psi_0(z)e^{-K_{||}z} \quad \text{(A5)}$$

may be thought of as a coupling constant. Finally, evaluating the time integral in Eq. (A4) yields

$$S=-\frac{8\pi i\gamma v\cos\theta}{(1+\epsilon_c)[(K_{||}v_z)^2+(\omega+\vec{K}_{||}\cdot\vec{v}_{||})^2]} . \quad \text{(A6)}$$

The differential scattering probability is

$$\frac{d^3\mathscr{P}}{d\omega\,d\vec{K}_{||}}=2\int\frac{d^2q_{||}}{(2\pi)^2}\int\frac{d^2q'_{||}}{(2\pi)^2}\Theta\left[\epsilon_F-\epsilon_0-\frac{q_{||}^2}{2m^*}\right]\Theta\left[\epsilon_1+\frac{q_{||}'^2}{2m^*}-\epsilon_F\right]\times|S|^2\delta^{(2)}(\vec{q}_{||}-\vec{q}\,'_{||}-\vec{K}_{||})\delta\left[\omega-\epsilon_1-\frac{q_{||}'^2}{2m^*}+\epsilon_0+\frac{q_{||}^2}{2m^*}\right]\cos\theta , \quad \text{(A7)}$$

where a factor of 2 has been included for the summation over spins. Further integration leads finally to

$$\frac{d^3\mathscr{P}}{d\omega\,d\delta\theta\,d\delta\phi}=\frac{\sin\theta\cos\theta}{2\epsilon}\left[\frac{8\pi\gamma v}{1+\epsilon_c}\right]^2\frac{D}{\left[(\sin\theta\,\delta\phi)^2+(\delta\theta)^2+\left[\frac{\delta\epsilon}{2\epsilon}\right]^2\right]^2} , \quad \text{(A8)}$$

where

$$D=\frac{1}{4\pi^4}\left[\frac{m^*}{K_{||}}\right]^2\Theta(y_2-y_1)\left\{\left[\frac{2K_{||}^2Y_2}{m^*}-\left[\omega+\epsilon_0-\epsilon_1-\frac{K_{||}^2}{2m^*}\right]^2\right]^{1/2}-\left[\frac{2K_{||}^2Y_1}{m^*}-\left[\omega+\epsilon_0-\epsilon_1-\frac{K_{||}^2}{2m^*}\right]^2\right]^{1/2}\right\} \quad \text{(A9)}$$

and

$$Y_1=\max\left[\epsilon_F-\epsilon_0-\omega,\frac{m^*}{2K_{||}^2}\left[\omega+\epsilon_0-\epsilon_1-\frac{K_{||}^2}{2m^*}\right]^2\right] , \quad \text{(A10a)}$$

and

$$Y_2=\epsilon_F-\epsilon_0 . \quad \text{(A10b)}$$

In order to evaluate the coupling constant γ appearing in Eqs. (A5) and (A8) a model for ψ_0 and ψ_1 is employed. We choose a nodeless form for ψ_0,

$$\psi_0(z)=Aze^{-\alpha z} , \quad \text{(A11a)}$$

and a single node form for ψ_1,

$$\psi_1(z)=Bz(1+bz)e^{-\beta z} . \quad \text{(A11b)}$$

The constants A, B, and b are fixed by orthonormality constraints. The constants α and β are fixed by using the Bates-Damgaard method of atomic physics. Thus

$$\alpha=[2m^*(V_s-\epsilon_0)]^{1/2} , \quad \text{(A12a)}$$

$$\beta=[2m^*(V_s-\epsilon_1)]^{1/2} , \quad \text{(A12b)}$$

$$A=2\alpha^{3/2} , \quad \text{(A12c)}$$

$$B=(2\beta)^{3/2}[2+6b/\beta+6(b/\beta)^2]^{-1/2} , \quad \text{(A12d)}$$

$$b=-(\alpha+\beta)/3 , \quad \text{(A12e)}$$

and

$$\gamma=2ABK_{||}(\alpha+\beta+K_{||})^{-4} . \quad \text{(A13)}$$

The final expression for the interband contribution is embodied in Eqs. (A8), (A9), and (A13). This must be integrated over the detector functions (15) and (19) before it can be compared with the plasmaron contributions.

[1]See, for example, Proceedings of the Fourth International Conference on Electronic Properties of Two-Dimensional Systems, New Hampshire, 1981, edited by F. Stern [Surf. Sci. 113, 1 (1982)].

[2]T. Ando, A. B. Fowler, and F. Stern, Rev. Mod. Phys. 54, 437 (1982).

[3]K. von Klitzing, G. Dorda, and M. Pepper, Phys. Rev. Lett. 45, 494 (1980).

[4]R. B. Laughlin, Phys. Rev. B 23, 5623 (1981).

[5]H. Ibach, Phys. Rev. Lett. 24, 1416 (1970); J. Vac. Sci. Technol. 9, 713 (1972).

[6]Y. Goldstein, A. Many, I. Wagner, and J. Gersten, Surf. Sci. 98, 599 (1980).

[7]A. Many, I. Wagner, A. Rosenthal, J. I. Gersten, and Y. Goldstein, Phys. Rev. Lett. 46, 1648 (1981).

[8]A. Many, J. I. Gersten, I. Wagner, A. Rosenthal, and Y. Goldstein, Surf. Sci. 113, 355 (1982).

[9]J. I. Gersten, Surf. Sci. 92, 579 (1980); 97, 206 (1980).

[10]See the review article by H. Froitzheim, in *Electron Spectroscopy for Surface Analysis,* Vol. 4 of *Topics in Current Physics,* edited by H. Ibach (Springer, Berlin, 1977), p. 205. Also see E. Evans and D. L. Mills, Phys. Rev. B 5, 4126 (1972); 7, 853 (1973); D. L. Mills, Surf. Sci. 48, 59 (1975).

[11]J. B. Pendry, *Low Energy Electron Diffraction* (Academic, New York, 1974).

[12]G. Heiland, E. Molwo, and F. Stockmann, in *Solid State Physics,* edited by H. Ehrenreich, F. Seitz, and D. Turnbull (Academic, New York, 1958), Vol. 8, p. 193.

[13]G. Heiland and P. Kuntsmann, Surf. Sci. 13, 72 (1969).

[14]Y. Goldstein, A. Many, D. Eger, Y. Grinshpan, G. Yaron, and M. Nitzan, Phys. Lett. 62A, 57 (1977).